LETTER

doi:10.1038/nature16176

Measurement noise 100 times lower than the quantum-projection limit using entangled atoms

Onur Hosten[1], Nils J. Engelsen[1], Rajiv Krishnakumar[1] & Mark A. Kasevich[1]

Quantum metrology uses quantum entanglement—correlations in the properties of microscopic systems—to improve the statistical precision of physical measurements[1]. When measuring a signal, such as the phase shift of a light beam or an atomic state, a prominent limitation to achievable precision arises from the noise associated with the counting of uncorrelated probe particles. This noise, commonly referred to as shot noise or projection noise, gives rise to the standard quantum limit (SQL) to phase resolution. However, it can be mitigated down to the fundamental Heisenberg limit by entangling the probe particles. Despite considerable experimental progress in a variety of physical systems, a question that persists is whether these methods can achieve performance levels that compare favourably with optimized conventional (non-entangled) systems. Here we demonstrate an approach that achieves unprecedented levels of metrological improvement using half a million ^{87}Rb atoms in their 'clock' states. The ensemble is 20.1 ± 0.3 decibels (100-fold) spin-squeezed via an optical-cavity-based measurement. We directly resolve small microwave-induced rotations 18.5 ± 0.3 decibels (70-fold) beyond the SQL. The single-shot phase resolution of 147 microradians achieved by the apparatus is better than that achieved by the best engineered cold atom sensors despite lower atom numbers[2,3]. We infer entanglement of more than 680 ± 35 particles in the atomic ensemble. Applications include atomic clocks[4], inertial sensors[5], and fundamental physics experiments such as tests of general relativity[6] or searches for electron electric dipole moment[7]. To this end, we demonstrate an atomic clock measurement with a quantum enhancement of 10.5 ± 0.3 decibels (11-fold), limited by the phase noise of our microwave source.

Quantum noise arises from the impossibility of simultaneously measuring conjugate physical observables. For example, for a harmonic oscillator, capturing the basic physics of light or superconducting circuits, the conjugate observables would be position and momentum. These observables exhibit finite uncertainties even in the lowest possible energy state. For an ensemble of N two-level atoms, a convenient mapping that captures the physics is the pseudo-spin system, where each atom is a spin-half system and the ensemble constitutes a spin-J system ($J = N/2$). The conjugate observables are the Cartesian spin components $J_{x,y,z}$ with the uncertainty relation $\Delta J_z \cdot \Delta J_y \geq |J_x/2|$, and can be pictorially represented on a Bloch sphere (see below). For an unentangled ensemble in a coherent spin state (CSS) with $\langle J_y \rangle = \langle J_z \rangle = 0$ the uncertainties are given by $\Delta J_z = \Delta J_y = \sqrt{N}/2$. This quantity is the projection noise of a CSS (CSS noise).

'Squeezing'[8] serves to redistribute the noise to make the observable of interest quieter than the CSS noise level, while still conforming to uncertainty relations. This process is non-classical as it introduces quantum entanglement into the system. The metrological improvement provided by squeezing is quantified by[9] $\chi^2 = \left(\frac{\sqrt{N}/2}{\Delta J_z} \cdot \frac{|J_x|}{N/2} \right)^2$; the first factor represents noise reduction, whereas the second represents coherence loss. This quantity translates directly into reduction in resources needed to perform a specific measurement (20 dB ($\chi^2 = 100$) is equivalent to a 100-fold increase in atom number or reduction in averaging time).

In optical settings[10] and superconducting microwave circuits[11], squeezing in excess of 12 dB has been demonstrated. Implementations in the interferometers of the GEO-600 and LIGO gravitational wave detectors achieved 2.5 dB improvements[12]. Other demonstrations include non-invasive biological imaging[13]. Spin-squeezing has been shown in cold atomic ensembles with methods based on both interaction[14–16] and measurement[17–19]. States squeezed by 5.6 dB (ref. 20) were used to obtain atomic-clock improvements up to 4.5 dB (ref. 21), and magnetometer enhancements up to 3.4 dB were observed in other experiments[22,23]. A metrological improvement of 10 dB was attained in a cavity-based experiment[24] taking advantage of cycling transitions in ^{87}Rb. However, as it utilizes magnetically sensitive states, and atoms are non-uniformly coupled to the cavity, this last approach is not suitable

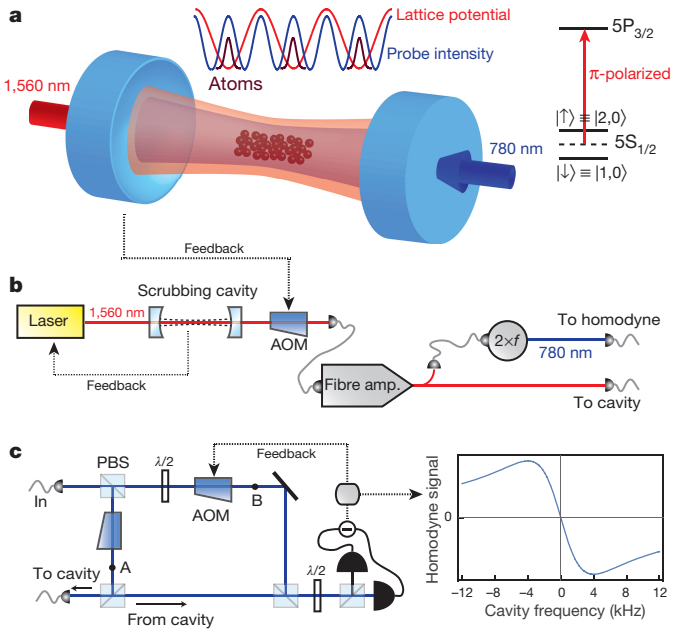

Figure 1 | Overall setup. a, Uniform atom–probe coupling: atoms are trapped at the maxima of the probe intensity profile by the 1,560 nm lattice (left). The 780 nm probe light is detuned by equal and opposite amounts from the two clock states (right). **b**, Probe light is generated by frequency-doubling the 1,560 nm light whose frequency is stabilized to match that of the main cavity resonance via feedback control. No further frequency stabilization of the probe is required, eliminating residual 780 nm light inside the cavity. AOM, acousto-optic modulator; PBS, polarizing beam-splitter. **c**, Homodyne detection system and the form of the output signal. Path 'A' contains two path length stabilizing side-bands, in addition to the probe frequency, also present on path 'B'. See Methods for details of **a**–**c**.

[1]Department of Physics, Stanford University, Stanford, California 94305, USA.

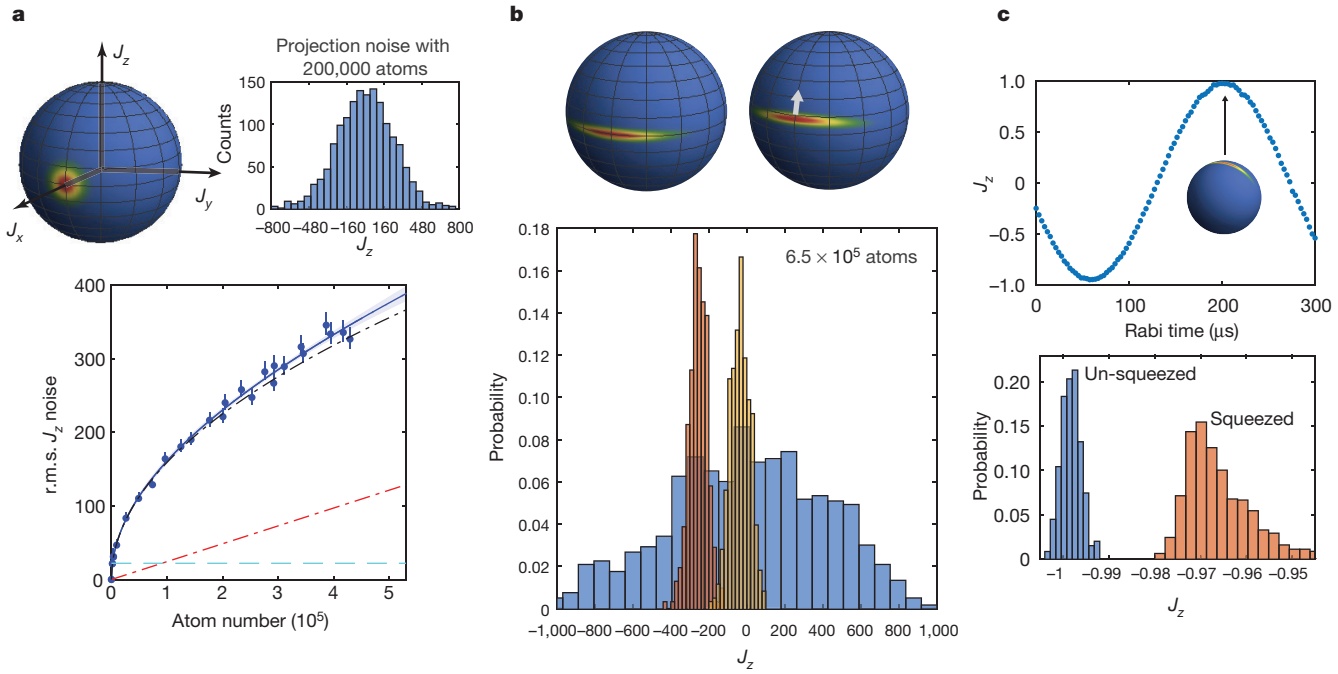

Figure 2 | Squeezing and metrology. a, Projection noise of unentangled spins. Top: pictorial representation of a CSS on Bloch sphere (left) and a sample J_z distribution (right). Bottom: characterization of CSS noise. Dot-dashed curve, the expected noise; solid line, fit revealing the underlying microwave rotation noise (dot-dashed straight line); dashed line, resolution of the π-strength measurement (subtracted in quadrature from the data). Error bars, 68% statistical confidence interval. **b**, Top: pictorial representation of two squeezed spin states, one rotated in the direction of the white arrow by a weak microwave pulse by 660 μrad. Bottom: the corresponding measured squeezed distributions overlaid on the un-squeezed distribution (measurement strengths, 0.75π–2.0π). **c**, Top: 96.2%-contrast Rabi oscillations executed by the squeezed state, observed with fluorescence imaging. The Bloch sphere represents the state at the indicated point. Bottom: measured J_z distributions at the lowest point of the Rabi oscillations. The width of the un-squeezed case, shown for reference, is limited by camera read-out noise.

for atomic clocks and other precision sensors requiring the release of trapped atoms from their locations in the cavity.

Owing to systematic errors arising from collisions between atoms, there is typically an upper bound to the number of atoms that can be employed in state-of-the-art cold atom sensors[2–4]. Squeezing offers a universal path to surpassing this limitation in sensitivity. However, methods demonstrated thus far have fallen significantly short of achieving competitive single-shot phase readout sensitivities.

Here we present a quantum metrology implementation using the magnetically insensitive clock states ($|\uparrow\rangle$ and $|\downarrow\rangle$) of ^{87}Rb (refs 19–21). We prepare the squeezed states through a collective population difference measurement on the atoms. In the spin language, we make a J_z measurement that projects the quantum state into one with a narrower distribution of J_z than that of a CSS. The measurement is enabled by a high-finesse optical cavity: the $|\downarrow\rangle$ ($|\uparrow\rangle$) atoms increase (decrease) the index of refraction seen by the probe light. Therefore, the frequency shift of the cavity resonance is a direct predictor of J_z.

The J_z measurement resolution is determined by the competition between photon shot noise and probe induced Raman scattering (spin-flips). The former limits the precision of the cavity frequency measurements; the latter leads to a random walk in the measured observable. For the ^{87}Rb clock states we expect an optimal enhancement of $\chi^2_{\rm opt} \approx \frac{\sqrt{3/2\,\varepsilon NC}}{1+NC(\Gamma/\omega_{\rm HF})^2}$ (see Methods and ref. 25). Here, C is the cooperativity (photon-scattering-rate ratio into cavity mode versus free-space), $\Gamma/\omega_{\rm HF}$ is the ratio between the excited state linewidth and the hyperfine splitting, and ε is the overall probe detection efficiency. The enhancement saturates with atom number owing to the impact of atomic absorption on measurement sensitivity, in addition to the spin-flips. For our parameters ($\varepsilon = 0.16$), the upper bound on achievable squeezing is about 24 dB.

We operate in a configuration where the probe light is uniformly coupled to all the atoms that are confined in a one-dimensional optical lattice (Fig. 1a). As we will elaborate, this uniform coupling will enable retrieval of squeezing even if the atoms are released from the optical lattice—a key requirement for many cold atom sensors. In contrast to earlier work[19–21,24], we prepare squeezed states without resorting to spin-echo techniques required for non-uniformly coupled systems, and we base squeezing levels on the true CSS noise level of N atoms (instead of an inferred level using lower effective numbers of atoms).

The core apparatus is described in ref. 26. We load the 520-μK-deep optical lattice with a 25 μK ensemble of up to 7×10^5 atoms prepared in the lower clock state (see Methods). Our 10.7-cm near-confocal cavity with a finesse of 1.75×10^5 (linewidth $\kappa_0 = 8.0$ kHz) yields $C = 0.78$. The cavity resonance frequency is measured with a homodyne detection system (Fig. 1b, c) that is limited by photon shot noise down to 10 Hz noise frequencies, well below the frequency range of interest (~0.2–4 kHz). The form of the signal is shown in Fig. 1c. The probe laser frequency is stable down to cavity shifts induced by three spin-flips. For reference, a spin-flip causes a 5.5 Hz shift, a value calculated from the well-known atom–cavity parameters, and verified experimentally at the 10% level with ac-Stark shift measurements for a known intra-cavity probe power.

We first calibrate our CSS noise level. With a π/2 microwave pulse we bring the state to the equator on the Bloch sphere. To suppress microwave pulse amplitude noise, the implementation is in two steps: $\pi/2_0 - \pi_{2\pi/3}$ (subscripts indicate relative phase between pulses). Subsequently, we probe the cavity with a 200 μs probe pulse (see Methods). We obtain a distribution of cavity shifts revealing the J_z distribution (Fig. 2a). Since we measure a balanced population difference, atom number fluctuations (~2% r.m.s.) between different runs do not enter at a measurable level. Microwave rotation noise becomes noticeable towards 5×10^5 atoms.

Next, we show that the J_z measurements indeed prepare a state with reduced J_z noise. Irrespective of the noise on the first measurement, a second measurement should be correlated (to within the measurement strength) with the first one. We quantify the measurement strength

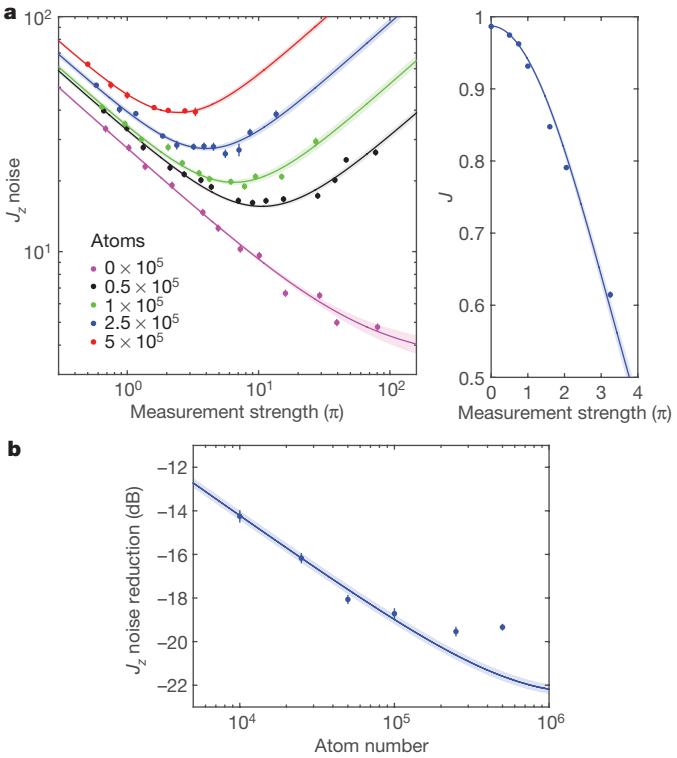

Figure 3 | Measured spin-noise reduction and coherence. a, Left: observed spin-noise (r.m.s.) for the difference between two equal-strength back-to-back measurements separated by 1.1 ms (half transverse oscillation period). No-atom data signifies the noise floor. Solid lines, model fits (see Methods). Right: Mean length J of the Bloch vector (coherence), obtained by measuring Ramsey fringe contrasts following the first measurement. Loss in coherence is due to lattice induced ac-Stark shifts which are partially cancelled by probe ac-Stark shifts. Solid line, Gaussian decay fit. **b**, Atom number dependence of maximum observed spin-noise reduction with respect to CSS noise (0 dB is no reduction). Solid line, model fit (see Methods). Error bars and shaded regions in all panels, 68% statistical confidence interval for data and fits respectively.

by the amount of differential phase shift (in radians) accumulated on the clock states due to probe-induced ac-Stark shifts. At high atom numbers, CSS noise exceeds the linear region of the homodyne signal. Outside this region both the measurement efficiency and the intra-cavity probe power decrease; the former degrades achievable squeezing, and the latter results in varying ac-Stark shifts. To remedy this problem, we start with states deterministically pre-squeezed up to 7 dB with 99% coherence (see Methods). Figure 3a shows the noise in the difference between two identical strength back-to-back measurements, as well as coherences, as a function of measurement strength (determined by incident probe power) for different atom numbers. Spin noise reductions at optimal measurement strengths saturate with atom number (Fig. 3b), albeit slightly earlier than expected, suggesting unknown sources of additional noise. States prepared by the first measurement are input states to any subsequent metrology experiment. Owing to the additional uncorrelated noise from the second measurement, these states contain 3 dB more squeezing than directly observed in the measurement difference (see ref. 19). The input state with the largest inferred metrological enhancement is at 5×10^5 atoms with a π measurement strength, which gives 20.1(3) dB (here the digit in parentheses represents the uncertainty in the final digit of the value) enhancement capability including the 0.6 dB loss from the measured 93.2% coherence. In Methods, we show that some of the prepared states contain in excess of 680(35) particle entanglement (following refs 27, 28), and also discuss the level of anti-squeezing in J_y.

To demonstrate a metrology example, we decrease the first measurement strength to 0.75π while increasing the second one to 2.0π.

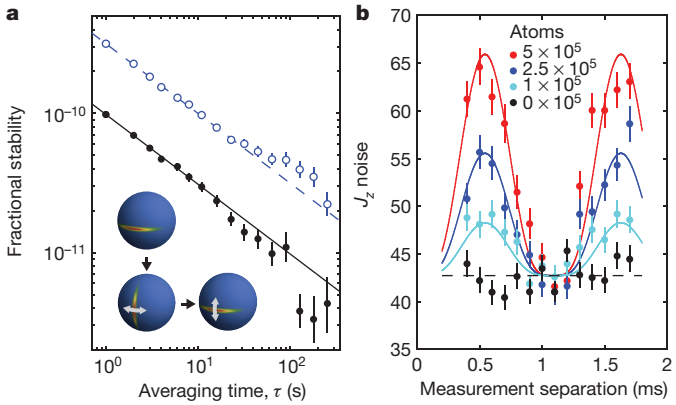

Figure 4 | Clock implementation. a, Allan deviation—a measure quantifying clock stability—of a squeezed atomic clock for 228 μs interrogation time at 1 Hz repetition rate (filled circles). The state is rotated into phase-sensitive orientation during the interrogation time. Dashed line, theoretical CSS noise limit; open circles, measured CSS noise level for the same Ramsey time. Solid line, $9.7 \times 10^{-11}\ s^{1/2}/\sqrt{\tau}$. The Bloch spheres illustrate the clock sequence with squeezed states; white arrows depict conversion of phase jitter into population jitter. **b**, Inhomogeneity analysis: back-to-back measurement noise as a function of measurement separation time. No matching pattern in mean J_z difference between the measurements is observed; only the noise is modulated. Measurement strengths are chosen to make the noise minima equal for different atom numbers. Solid lines are predictions with no free parameters. Error bars in both panels, 68% statistical confidence interval.

In this configuration, coherence after the first measurement is 96.2% (with 2×10^{-3} photons per atom free-space scattering), and the second measurement recovers more information. We obtain a directly measured metrological improvement of 18.5(3) dB with respect to the SQL, with which we resolve small rotations around J_y at 6.5×10^5 atoms (Fig. 2b, c). This corresponds to 147 μrad (r.m.s.) single-shot phase sensitivity.

To take full advantage of the achieved sensitivity for implementing an atomic clock, we need to reduce the phase noise of our microwave local oscillator. Nevertheless, here we include a preliminary clock demonstration. In particular, we show that we can compare the atomic and microwave phases to better than that allowed by CSS noise. Following J_z-squeezing, we apply a $\pi/2$ pulse (74 μs) to rotate the noise ellipse into a phase-sensitive state, then wait for phase accumulation, and finally map this phase onto J_z with another rotation (Fig. 4a inset). High-frequency microwave phase noise during the measurement interrogation period results in excess noise proportional to the atom number. To obtain the maximum quantum enhancement, we lower the atom numbers to 1×10^5 and observe up to 10.5(3) dB metrological gain in phase comparison. To put these measurements in context with clock performance[21], we operate with the largest Ramsey time (~228 μs phase accumulation) which does not measurably degrade the comparison. We achieve 9.7×10^{-11} fractional stability at 1 s averaging time (Fig. 4a). For the fixed Ramsey time, the squeezed clock reaches a given precision 11.2(8) times faster than possible without squeezing. High-frequency local oscillator phase noise can be circumvented using interleaved clocks[29], in which case the full advantage of squeezing can be achieved using adaptive measurements[30].

The squeezed states prepared in this work can be released from the confining lattice for precision sensing applications. To infer the retrievable squeezing in a configuration where the second cavity measurement is replaced with fluorescence imaging in free space, we analyse the noise modulations observed in back-to-back cavity measurements (Fig. 4b) as a function of delay time between the measurements. These modulations are evidently due to residual atom–probe coupling inhomogeneities, and on the basis of our model, we anticipate retrieving up to 14.6 dB squeezing (see Methods).

Online Content Methods, along with any additional Extended Data display items and Source Data, are available in the online version of the paper; references unique to these sections appear only in the online paper.

Received 30 June; accepted 22 October 2015.

Published online 11 January 2016.

1. Giovannetti, V., Lloyd, S. & Maccone, L. Quantum-enhanced measurements: beating the standard quantum limit. *Science* **306,** 1330–1336 (2004).
2. Guéna, J., Abgrall, M., Clairon, A. & Bize, S. Contributing to TAI with a secondary representation of the SI second. *Metrologia* **51,** 108–120 (2014).
3. Rocco, E. *et al.* Fluorescence detection at the atom shot noise limit for atom interferometry. *New J. Phys.* **16,** 093046 (2014).
4. Bloom, B. J. *et al.* An optical lattice clock with accuracy and stability at the 10^{-18} level. *Nature* **506,** 71–75 (2014).
5. Geiger, R. *et al.* Detecting inertial effects with airborne matter-wave interferometry. *Nature Commun.* **2,** 474 (2011).
6. Gaaloul, N. *et al.* Quantum tests of the equivalence principle with atom interferometry. *Acta Astronaut.* **67,** 1059–1062 (2010).
7. Weiss, D. S., Fang, F. & Chen, J. Measuring the electric dipole moment of Cs and Rb in an optical lattice. *Bull. Am. Phys. Soc.* **APR03,** J1.008 (2003).
8. Kitagawa, M. & Ueda, M. Squeezed spin states. *Phys. Rev. A* **47,** 5138–5143 (1993).
9. Wineland, D. J., Bollinger, J. J., Itano, W. M. & Heinzen, D. J. Squeezed atomic states and projection noise in spectroscopy. *Phys. Rev. A* **50,** 67–88 (1994).
10. Eberle, T. *et al.* Quantum enhancement of the zero-area Sagnac interferometer topology for gravitational wave detection. *Phys. Rev. Lett.* **104,** 251102 (2010).
11. Eichler, C., Salathe, Y., Mlynek, J., Schmidt, S. & Wallraff, A. Quantum-limited amplification and entanglement in coupled nonlinear resonators. *Phys. Rev. Lett.* **113,** 110502 (2014).
12. The LIGO Scientific Collaboration. A gravitational wave observatory operating beyond the quantum shot-noise limit. *Nature Phys.* **7,** 962–965 (2011).
13. Taylor, M. A. *et al.* Biological measurement beyond the quantum limit. *Nature Photon.* **7,** 229–233 (2013).
14. Gross, C., Zibold, T., Nicklas, E., Esteve, J. & Oberthaler, M. K. Nonlinear atom interferometer surpasses classical precision limit. *Nature* **464,** 1165–1169 (2010).
15. Riedel, M. F. *et al.* Atom-chip-based generation of entanglement for quantum metrology. *Nature* **464,** 1170–1173 (2010).
16. Hamley, C. D., Gerving, C. S., Hoang, T. M., Bookjans, E. M. & Chapman, M. S. Spin-nematic squeezed vacuum in a quantum gas. *Nature Phys.* **8,** 305–308 (2012).
17. Appel, J. *et al.* Mesoscopic atomic entanglement for precision measurements beyond the standard quantum limit. *Proc. Natl Acad. Sci. USA* **106,** 10960–10965 (2009).
18. Takano, T., Fuyama, M., Namiki, R. & Takahashi, Y. Spin squeezing of a cold atomic ensemble with the nuclear spin of one-half. *Phys. Rev. Lett.* **102,** 033601 (2009).
19. Schleier-Smith, M. H., Leroux, I. D. & Vuletic, V. States of an ensemble of two-level atoms with reduced quantum uncertainty. *Phys. Rev. Lett.* **104,** 073604 (2010).
20. Leroux, I. D., Schleier-Simith, M. H. & Vuletic, V. Implementation of cavity squeezing of a collective atomic spin. *Phys. Rev. Lett.* **104,** 073602 (2010).
21. Leroux, I. D., Schleier-Smith, M. H. & Vuletic, V. Orientation-dependent entanglement lifetime in a squeezed atomic clock. *Phys. Rev. Lett.* **104,** 250801 (2010).
22. Sewell, R. J., Koschorreck, M., Napolitano, M., Dubost, B. & Mitchell, M. W. Magnetic sensitivity beyond the projection noise limit by spin squeezing. *Phys. Rev. Lett.* **109,** 253605 (2012).
23. Muessel, W., Strobel, H., Linnemann, D., Hume, D. B. & Oberthaler, M. K. Scalable spin squeezing for quantum-enhanced magnetometry with Bose-Einstein condensates. *Phys. Rev. Lett.* **113,** 103004 (2014).
24. Bohnet, J. G. *et al.* Reduced spin measurement back-action for a phase sensitivity ten times beyond the standard quantum limit. *Nature Photon.* **8,** 731–736 (2014).
25. Chen, Z., Bohnet, J. G., Weiner, J. M., Cox, K. C. & Thompson, J. K. Cavity-aided nondemolition measurements for atom counting and spin squeezing. *Phys. Rev. A* **89,** 043837 (2014).
26. Lee, J., Vrijsen, G., Teper, I., Hosten, O. & Kasevich, M. Many-atom–cavity QED system with homogeneous atom–cavity coupling. *Opt. Lett.* **39,** 4005–4008 (2014).
27. Sørensen, A. S. & Mølmer, K. Entanglement and extreme spin squeezing. *Phys. Rev. Lett.* **86,** 4431–4434 (2001).
28. Lücke, B. *et al.* Detecting multiparticle entanglement of Dicke states. *Phys. Rev. Lett.* **112,** 155304 (2014).
29. Biedermann, G. W. *et al.* Zero-dead-time operation of interleaved atomic clocks. *Phys. Rev. Lett.* **111,** 170802 (2013).
30. Borregaard, J. & Sørensen, A. S. Near-Heisenberg-limited atomic clocks in the presence of decoherence. *Phys. Rev. Lett.* **111,** 090801 (2013).

Acknowledgements We thank I. Teper, G. Vrijsen and J. Lee for technical contributions to the experiment. This work was support by DTRA, an NSSEFF fellowship and the ONR.

Author Contributions O.H., N.J.E., R.K. and M.A.K. carried out the experiment, analysed the data, and prepared the manuscript.

Author Information Reprints and permissions information is available at www.nature.com/reprints. The authors declare no competing financial interests. Readers are welcome to comment on the online version of the paper. Correspondence and requests for materials should be addressed to M.A.K. (kasevich@stanford.edu).

METHODS

Squeezing measurement details. The incident probe laser power is always increased and decreased adiabatically. The duration of the measurement pulses is 200 μs—the shortest possible time while avoiding significant ringing in the homodyne signal. Typical incident probe powers are of the order of 10 pW (intra-cavity photon numbers: 90 photons per pW on resonance). Since the homodyne signal is time dependent, we apply a time-dependent weighting function in the analysis of the time traces to extract the cavity frequency shift. This method gives the same signal and photon shot noise values irrespective of pulse shapes and duration as long as the pulse area is conserved and the intra-cavity power adiabatically follows the incident power. Quantitatively, given a time-dependent homodyne signal $s(t)$, the cavity shift is $\Delta\nu = D\int \mathrm{d}t\ s(t)\rho(t)/\int \mathrm{d}t\ \rho^2(t)$, where D is the frequency discriminator (Hz/V) at the peak signal level, and $\rho(t)$ is the temporal shape of the signal normalized such that its peak is at 1. $\rho(t)$ and D are determined experimentally in the absence of atoms by detuning the probe from the exact cavity resonance by a small amount (well within cavity linewidth), and recording the homodyne signal.

The procedure above extracts the correct cavity shift as long as the homodyne signal is in the linear regime. We apply an additional correction factor to properly measure the shifts which are outside this linear regime. This factor is calibrated by setting the cavity–probe detuning to a known value and noting the discrepancy between the known shift and the inferred shift. This is important when establishing CSS noise levels.

At large atom numbers the cavity linewidth broadens owing to atomic scattering, causing the squeezing saturation. The atom-number-dependent linewidth is $\kappa = \kappa_0 + \kappa_S$, with κ_0 the empty cavity linewidth and κ_S the additional scattering contribution. The fractional change is $\kappa_S/\kappa_0 = NC(\Gamma/\omega_{HF})^2$. We incorporate this signal degrading effect into the cavity shift analysis. The change in the overall signal shape due to broadening is negligible for our parameter range. We experimentally verify that we indeed obtain $\kappa_S/\kappa_0 \approx 0.30$ at 5×10^5 atoms. To do this, we jump the cavity frequency by a known amount (smaller than κ) between consecutive measurements and observe the signal reduction in comparison to the empty cavity case. This measurement takes 10 min; it would have taken 11 h to reach the same precision had we not employed squeezed states.

Homodyne detection system. The homodyne detection setup (Fig. 1c) is seeded with 780 nm light obtained by frequency doubling the 1,560 nm lattice light, which is frequency stabilized to the main cavity following an intermediate stabilization step involving a scrubbing cavity (to narrow down the linewidth of the laser). Thus, the 780 nm light is already stable in the short-term with respect to the cavity (80 mHz/$\sqrt{\text{Hz}}$ level in the 0.2–4 kHz band—about 8 Hz (r.m.s.) stability). In the long term, thermal drifts in the cavity mirror coatings cause variations in the individual cavity lengths seen by the 780 nm and 1,560 nm light. During experimental cycles of 1 s, the probe frequency can drift by 100 Hz (r.m.s.); we correct the drift at the end of every cycle with an auxiliary empty cavity measurement.

Using a 200 μW local oscillator (shifted by 80 MHz from input) on path A of the homodyne system, the balanced detectors operate photon shot-noise limited from 10 Hz up to 5 MHz. Two 10 nW spectral components on path B (offset by 78 MHz and 82 MHz from input) travel to the cavity and promptly reflect back from the first mirror to give a heterodyne beat-note signal (2 MHz) at the detectors. This signal is used to stabilize the interferometer path lengths via feedback onto the AOM on path A. Stabilization covers the DC to 15 kHz frequency band, thus removing the influence of optical phase noise for the squeezing measurements. Path B also contains the probe (80 MHz offset from input), interfering with the local oscillator to form the homodyne signal after returning from the cavity.

The overall detection efficiency limiting the achievable squeezing is $\varepsilon = 0.16$. The breakdown is as follows: a factor of 0.50, since we collect light only from one cavity mirror; 0.57 due to loss in cavity mirrors; 0.80 backwards fibre coupling efficiency; 0.85, loss in isolator and other optical elements; 0.85, interferometer mode matching efficiency. Multiplying these factors results in the stated overall efficiency.

Our ability to estimate the centroid of the cavity resonance frequency improves with the square root of the number of photons contained in a 200 μs measurement pulse, and saturates around 15 Hz owing to laser frequency instability.

Inhomogeneity analysis for free-space release. Although we have uniform atom–cavity coupling, we still have residual inhomogeneities due to thermal motion. Figure 4b shows the noise between back-to-back measurements for varying measurement separations: noise is smallest when the separation is half-integer multiples of the 2.2 ms transverse-oscillation period. We model this behaviour to make an estimate of retrievable squeezing with fluorescence imaging.

The observed effect can be explained with the statistical fluctuations in atomic positions from one experimental cycle to the next. A classical trajectory analysis on the atoms in a harmonic trap (transverse motion) suffices to predict the noise in two consecutive cavity measurements as a function of measurement separation time. Given their initial phase space points during the first measurement, the location of the atoms during the second measurement, and hence the cavity frequency difference, can be deterministically predicted. However, each time the experiment is repeated, the atoms will start at a different configuration in phase space giving rise to a slightly different cavity frequency difference. We calculate this additional noise assuming a thermal distribution for the atoms. The resulting prediction is $\langle\Delta J_z^2\rangle^{1/2} = \sqrt{N}(1+\alpha^2)\left(\frac{1}{1+2\alpha^2} + \frac{1}{1+2\alpha^2+\alpha^4(1-\cos^4\omega t)} - \frac{2}{1+2\alpha^2+\alpha^4\sin^2\omega t}\right)^{1/2}$, where ω is the transverse oscillation angular frequency and $\alpha = 2\sigma_r/w_{780}$ with σ_r the transverse size of the atomic cloud and w_{780} the probe beam waist ($\alpha^2 = 0.076$). The solid lines in Fig. 4b are the addition of this function in quadrature with the baseline without any free parameters.

A similar analysis could be used to predict the additional noise that will arise when the first measurement is done using the cavity and the second one using fluorescence imaging. The second measurement is insensitive to atomic positions; hence the noise comes only from the statistical fluctuations in atomic positions during the first measurement. The estimate for the additional noise is $\langle\Delta J_z^2\rangle^{1/2} = \sqrt{N}\alpha^2/\sqrt{1+2\alpha^2}$, which is 17 dB below CSS noise for our experiment. In particular, an 18.5 dB squeezed state would read 14.6 dB with fluorescence imaging.

Atom/cavity parameters. For transitions from the clock states with π-polarized light, the single atom cooperativity is $C = 4g^2/\kappa_0\Gamma = 0.78$, with atom–cavity coupling $g = 2\pi\times 96.7$ kHz, empty cavity decay rate $\kappa_0 = 2\pi\times 8.0$ kHz, and atomic decay rate $\Gamma = 2\pi\times 6.06$ MHz. The value for g^2 is an average over the position distribution of the atoms inside the lattice due to the finite temperature. The 25 μK atoms are distributed over about 1,000 lattice sites. The r.m.s. atomic cloud size inside each 520-μK-deep lattice site is 17 μm in the transverse direction and 37 nm in the axial direction. The trap frequencies in the corresponding directions are 460 Hz and 205 kHz. We vary the atom number in the experiment by changing the initial magneto-optical trap (MOT) loading time. Strictly speaking, the residual inhomogeneity in atom–cavity coupling due to thermal motion requires one to define effective atom numbers N_{eff} for the purpose of identifying the CSS noise level. This method was adopted in refs 19, 20, 21 and 24, owing to lack of homogeneity in couplings, resulting in $N_{\text{eff}} \approx 0.66N_0$, with N_0 denoting the real atom number. In this work we achieve $N \equiv N_{\text{eff}} \approx 0.995N_0$ (see next section for details). For practical purposes, we do not differentiate between real and effective atoms.

Coupling inhomogeneity. We would like to measure the collective observable $J_z = \sum_{n=1}^{N_0} j_z^{(n)}$, with N_0 the total number of atoms, and $j_z^{(n)} = \frac{1}{2}\sigma_z^{(n)}$ the z-component of the spin operator for atom n. However, because of the residual inhomogeneity in the atom–cavity coupling we measure a slightly different collective observable J_z' that is a weighted sum over $j_z^{(n)}$.

If all atoms coupled identically to the cavity with the per-spin-flip cavity frequency shift for atom n given by $\delta^{(n)} = \delta_0$, the total shift would be $\Delta_0 = \sum_n \delta_0 j_z^{(n)} = \delta_0 J_z$. However, owing to the small fractional deviations ε_n in the coupling constants for the atoms n, the total shift is given by:

$$\Delta = \sum_n \delta^{(n)} j_z^{(n)} = \sum_n \delta_0(1-\varepsilon_n) j_z^{(n)} = (\delta_0 Z)\left(\frac{1}{Z}\sum_n (1-\varepsilon_n) j_z^{(n)}\right) \equiv \delta_{\text{eff}} J_z'$$

Here Z is a normalization constant, and $\delta_{\text{eff}} = \delta_0 Z$ is the effective cavity shift per spin flip. To decide on a normalization, we utilize two properties of J_z': its maximum $(J_z')_{\max} = \frac{N_0}{2}\frac{1}{Z}\langle 1-\varepsilon\rangle_e$ and its projection noise with uncorrelated atoms $\text{var}(J_z')_{\text{proj}} = \frac{N_0}{4}\frac{1}{Z^2}\langle(1-\varepsilon)^2\rangle_e$. Here $\langle\bullet\rangle_e$ indicates an ensemble average. We choose Z such that the statistical condition $\frac{\text{var}(J_z)}{(J_z)_{\max}} = \frac{N_0/4}{N_0/2} = \frac{1}{2}$ satisfied by J_z is also satisfied by J_z'. This leads to $Z = \frac{\langle(1-\varepsilon)^2\rangle_e}{\langle 1-\varepsilon\rangle_e}$, and thus:

$$J_z' = \frac{\langle 1-\varepsilon\rangle_e}{\langle(1-\varepsilon)^2\rangle_e}\sum_n (1-\varepsilon_n) j_z^{(n)}$$

Consequently, one can think of the non-uniformly coupled system of N_0 atoms as a uniformly coupled system of $N \equiv N_{\text{eff}} = N_0\frac{\langle 1-\varepsilon\rangle_e^2}{\langle(1-\varepsilon)^2\rangle_e} = 0.995N_0$ effective atoms in conjunction with an effective cavity shift $\delta_{\text{eff}} = \delta_0\frac{\langle(1-\varepsilon)^2\rangle_e}{\langle 1-\varepsilon\rangle_e} = 0.93\delta_0$ per spin-flip. Here δ_0 is the cavity shift for an atom on the cavity axis averaged over the distribution along the tightly trapped longitudinal direction. This gives $\delta_{\text{eff}} = 0.83\delta_{\max} = 5.5$ Hz, where $\delta_{\max}$ is the cavity shift for an atom localized at a peak of the probe mode profile.

Fluorescence imaging. Using the cavity, we detect J_z only in a very narrow range. For observing J_z in its full range of $\pm N/2$ we use fluorescence imaging. We release

the atoms from the lattice, and for state selectivity, we apply a laser beam resonant with the $F=2$ to $F'=3$ transition to momentarily push the $F=2$ (that is, $|\uparrow\rangle$) atoms. This spatially separates the $|\uparrow\rangle$ and $|\downarrow\rangle$ states, permitting the simultaneous detection of the number of atoms in both states. We image the fluorescence from the two clouds for 2 ms on a CCD camera using the cooling and re-pumping lights of the MOT. This is how the observed Rabi and Ramsey fringes are mapped out and hence how the coherence is measured.

The pre-squeezing procedure. The pre-squeezing procedure is a supplement to the J_z measurement protocol, increasing robustness and efficiency. However we note that it does not alter the nature of J_z measurements—we obtain the same final squeezing results in the absence of pre-squeezing if we post-select the runs with the first measurement outcome lying within the linear regime of the homodyne signal.

When approaching the saturated regime of squeezing, discussed in the main text, the r.m.s. cavity shifts due to CSS noise approach the linewidth of the cavity. This quantum noise prevents us from preparing initial J_z distributions that fall purely within the linear region of the homodyne signal using microwave rotations alone. We therefore resort to atom–cavity nonlinearities to deterministically pre-squeeze the state by a sufficient amount such that the distribution fits within the linear regime. The nonlinearity employed is a J_z^2 interaction causing one-axis twisting, similar to the one used in ref. 20. For an initial state near the J_x axis, the procedure dynamically compresses the distribution on the Bloch sphere in the z direction while expanding it in the y direction. The technical noise on the initial J_z preparation is also suppressed. The pre-squeezing occurs after the composite $\pi/2$ pulse brings the state to the equator. We send 100 nW of light at $6.25\kappa_0$ detuning from the bare cavity resonance (generating J_z^2 interaction) and simultaneously turn on a 400 μs microwave $\pi/12$ pulse (generating rotations around the J_x axis). With the combined action, we observe up to 7 dB unconditional J_z squeezing while retaining 99% coherence.

Amount of anti-squeezing. The cavity measurements, while projecting the atomic ensemble onto a state with reduced J_z noise, also act back onto the conjugate observable J_y and increase its noise. In the ideal case a measurement would preserve the area of the uncertainty ellipse, that is, the reduction and the increase in the noises of J_z and J_y respectively would be through the same factor. However owing to photon losses, inefficiencies in extracting the information in the readout, and the additional spin-flip noise in J_z, the balance is expected to be broken. Experimentally, the variance of J_y scales linearly with measurement strength, reaching 39 dB above CSS noise at π measurement strength accompanying the quoted 20.1(3) dB squeezing in J_z. This corresponds to a factor of 8.8 increase in the uncertainty ellipse area. The observed level of anti-squeezing is within 2 dB of the expectations.

Squeezing limits calculation. The maximum attainable spin noise reduction can be found by considering the individual effects of the measurement noise and the spin-flip noise. We will specify these quantities as functions of the (experimentally accessible) differential phase shift $\phi_{\mathrm{AC}}=\frac{2g^2}{\Delta}\int \mathrm{d}t\ n_{\mathrm{c}}(t)$ accumulated on the clock states. Here, $n_{\mathrm{c}}(t)$ is the intra-cavity photon number. We will also use the cooperativity, $C=\frac{4g^2}{\kappa_0\Gamma}$.

The number of scattered photons is $m_{\mathrm{s}}=\phi_{\mathrm{AC}}(\Gamma/\omega_{\mathrm{HF}})$. The hyperfine splitting enters because the atom–cavity detuning is set to $\Delta=\omega_{\mathrm{HF}}/2$. Using the branching ratios for ^{87}Rb, it can be shown that only 1/6 of the scattering events will give rise to a spin-flip, that is, a change of the hyperfine state. These spin-flips will give rise to a random walk on J_z with a variance of $\delta^2_{\mathrm{flip}}=\frac{N}{6}\frac{\Gamma}{\omega_{\mathrm{HF}}}\phi_{\mathrm{AC}}$. This is the spin-flip noise; it grows with atom number and probe power.

To examine the measurement noise, we analyse the information imprinted on the light transmitted from the cavity. The total decay rate of the cavity is $\kappa=2\kappa_{\mathrm{M}}+\kappa_{\mathrm{L}}+\kappa_{\mathrm{S}}$, where κ_{M} is due to mirror out-coupling, and κ_{L} is due to optical losses in the mirrors. The term due to atomic scattering can be expressed as $\kappa_{\mathrm{S}}/\kappa_0=NC(\Gamma/\omega_{\mathrm{HF}})^2$, where $\kappa_0=2\kappa_{\mathrm{M}}+\kappa_{\mathrm{L}}$. Around zero cavity–probe detuning, the number of photons transmitted through the cavity is $n_{\mathrm{T}}=\frac{\varepsilon_{\mathrm{c}}\,(\omega_{\mathrm{HF}}/\Gamma)}{2C}\phi_{\mathrm{AC}}$, where $\varepsilon_c=2\kappa_{\mathrm{M}}/\kappa_0$ is the cavity efficiency incorporating the optical losses. As the atoms shift the cavity frequency by $\frac{2g^2}{\Delta}J_z$, the phase shift on the light upon transmission is $\varphi=\frac{2C\ (\Gamma/\omega_{\mathrm{HF}})}{1+NC(\Gamma/\omega_{\mathrm{HF}})^2}J_z$. Given the quantum phase noise $\frac{1}{2\sqrt{n_{\mathrm{T}}}}$ for a coherent state, the noise equivalent J_z resolution is $\frac{1+NC(\Gamma/\omega_{\mathrm{HF}})^2}{\sqrt{8\varepsilon_{\mathrm{c}}C\ (\Gamma/\omega_{\mathrm{HF}})}}\frac{1}{\sqrt{\phi_{\mathrm{AC}}}}$. For a symmetric cavity, equal amounts of information leak out from each mirror. Thus, including the information gained from the reflection would improve the resolution by $\sqrt{2}$. Lastly, we also include the effect of photon losses on the way to the detectors, and bundle all efficiency factors into the quantity ε which is further discussed in the 'Atom/cavity parameters' section above. The final expression for the measurement noise is $\delta^2_{\mathrm{meas}}=\frac{(1+NC(\Gamma/\omega_{\mathrm{HF}})^2)^2}{16\varepsilon C\ (\Gamma/\omega_{\mathrm{HF}})}\frac{1}{\phi_{\mathrm{AC}}}$; it decreases with increasing probe power.

As a first approximation, the total noise in the estimation of J_z can be found by adding the contribution due to the two sources: $\delta^2=\delta^2_{\mathrm{meas}}+\delta^2_{\mathrm{flip}}$. An optimal ϕ_{AC} (that is, measurement strength) minimizes this expression, at which point $\delta^2=\frac{\sqrt{N}(1+NC(\Gamma/\omega_{\mathrm{HF}})^2)}{\sqrt{24\varepsilon C}}$. Assuming negligible coherence loss, as is the case experimentally, we arrive at an optimal metrological enhancement $\chi^2_{\mathrm{opt}}=\frac{\sqrt{\varepsilon NC\ 3/2}}{1+NC(\Gamma/\omega_{\mathrm{HF}})^2}$. At first, the achievable enhancement increases with atom number, attaining a maximum of $(\omega_{\mathrm{HF}}/\Gamma)\sqrt{3\varepsilon/8}$ at $N_{\mathrm{opt}}=\omega^2_{\mathrm{HF}}/\Gamma^2C$. This saturation effect can be traced back to cavity linewidth broadening from atomic absorption. For $\varepsilon=1$, the maximum achievable enhancement is around 28 dB.

Exact numerical agreement should not be expected between the naive model presented here and the experiment, since the latter is more complicated. We use the functional forms derived here to fit to the data in Fig. 3. In particular, for Fig. 3a we use $\delta^2=\frac{\alpha}{\phi_{\mathrm{AC}}}+\beta\phi_{\mathrm{AC}}$, and for Fig. 3b we use $\chi^2_{\mathrm{opt}}=\gamma\frac{\sqrt{NC}}{1+NC(\Gamma/\omega_{\mathrm{HF}})^2}$. Here, α, β and γ are the fit parameters.

Entanglement depth. Measurements of the collective spin operators $J_i=\sum_{n=1}^{N}j_i^{(n)}$ for an ensemble of N two-level atoms can be used to quantify the amount of entanglement in the ensemble[27,28] without further reference to the specific nature of the states. We will follow the analysis of ref. 28, where the J_z variance and the mean-square Bloch vector length places the measured states on a plane with boundaries corresponding to different entanglement depths.

In our experiment, because of the residual inhomogeneities in atom–cavity coupling, we measure the collective observable $J'_z=\frac{1}{Z}\sum_{n=1}^{N}(1-\varepsilon_n)j_z^{(n)}$, where Z is a normalization constant and ε_n is the small fractional deviation in coupling for atom n (see 'Coupling inhomogeneity' section). This implies that we cannot directly utilize the measured spin noise values for the purposes of calculating entanglement depths. However, even without a direct measurement of J_z itself, its maximum possible variance can be inferred, as was argued in the Methods section 'Inhomogeneity analysis for free-space release'. There, we found that there would be an additive noise of 17 dB below CSS noise if we tried to read out the prepared states via fluorescence imaging, which we consider to be a true J_z measurement. Therefore, we infer J_z on the basis of this analysis. Unlike the cavity-based measurements, the Bloch vector length measurements, which are done via fluorescence imaging, can directly be used for calculating entanglement depths.

In Extended Data Fig. 1, we plot the inferred J_z variances for the 5×10^5 atom data set using the experimentally established noise after the first measurement ($\frac{1}{\sqrt{2}}$ of the values in Fig. 3a). The point with the largest metrological gain (π measurement strength) gives an entanglement depth of 330(15) atoms, while the largest entanglement depth is 680(35) (0.5π measurement strength) atoms. This exemplifies that entanglement depth is in itself not a direct predictor for metrological improvement.

The additional noise in our model in inferring J_z originates from shot-to-shot randomization of atomic positions. In the absence of this randomization, we expect the discrepancy between the variances of J'_z and J_z to be less. Thus, the quoted entanglement depths should be taken as lower bounds. For reference, had we not taken into account the coupling inhomogeneity we would have found the largest entanglement depth to be 1,605(30) atoms.

Sample size. No statistical methods were used to predetermine sample size.

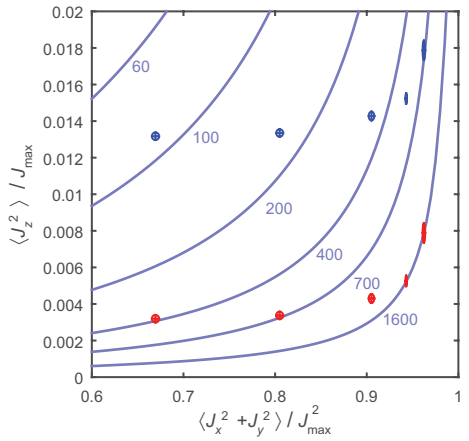

Extended Data Figure 1 | Inferred entanglement depths, quantifying multi-particle entanglement. The inferred spin noise variance (y axis) and the mean-square Bloch vector lengths (x axis) are plotted for the 5×10^5 atom data set. Note that the probe power decreases from left to right. The x-axis values are conservatively chosen to be the most probable value of the measured Bloch vector length distributions (Fig. 2c). A state below an M-particle boundary (purple lines labelled with particle numbers) is guaranteed to contain at least groups of M particles whose quantum states are non-separable. The blue data set establishes a lower bound on entanglement depth taking into account the residual inhomogeneity in atom–cavity coupling. The red data set, for reference, shows what we would have obtained had we ignored the small inhomogeneity. The ellipses correspond to the 68% statistical confidence intervals on the quoted values. $J_{\max} = N/2$. The third data point in each set shows the largest metrological improvement.